

An atmospheric gravitational vortex as a flow object: improvement of the three-layer model

Sandro Nižetić

Department of Thermodynamics, Thermotechnics and Heat Engines, Faculty of Electrical Engineering, Mechanical Engineering and Naval Architecture, University of Split

Received 26 May 2009, in final form 24 November 2009

An improved physical and analytical three-layer model of gravitational vortex columns (GVCs) for solar chimney power plants is developed in this paper. In essence, this model represents a further improvement and upgrade of the three-layer model proposed in Ninić et al. (2009). The improvements of the three-layer model deal with internal friction, variable vertical velocity (by height) in the central GVC spiraling upward flow, and variable angular momentum of the downdraft shell. A numerical solution of the improved model is given as a characteristic case and is compared to the elementary GVC model. The results show that the introduced improvements are important parameters for further analysis of gravitational vortex columns.

Keywords: Gravitational vortex, solar chimney, numerical modelling

1. Introduction

The concept of the gravitational vortex column (GVC) for solar chimney power plants was proposed in Ninić (2006). An elementary model of a stationary GVC was developed by Ninić et al. (2009). The solar chimney power plant (SC) was originally proposed by J. Schlaich in 1968, and represents the basis for the further extension of the GVC concept. Solar chimneys have been extensively studied; see, for example, Haff et al. (1983), Haff (1984), Padki and Sherif (1989), Schlaich (1995), Bernardes et al. (2003), Backström von T.W. (2006), Bilgen (2005) and Nižetić et al. (2007, 2008 and 2009). A detailed literature review of this field was given in Bernardes et al. (2003).

The idea of using an atmospheric gravitational vortex as a flow object is not a new one. It was originally presented in Dessoliers (1913). Dessens (1962, 1969) performed an experiment that proved such an idea in principle. Michaud (1975) proposed a “vortex power station” and also developed his idea in later papers, including Michaud (1995, 1999). The same author also performed a simple experiment as a validation of his assumptions. These papers demonstrated the potential for the technical utilization of the working availability of

warm moist air (i.e., the technically feasible part). Namely, the technically feasible part of working availability is equivalent to the work of the buoyancy force affecting 1 kg of air that has left the collector. Michaud (1995), Michaud (1996), Ninić (2006) and Ninić et al. (2006) dealt with the magnitude of warm moist air's working availability in the atmosphere.

Furthermore, Michaud (1975) and Ninić and Nižetić (2007) considered the possibility of the technical utilization and the controlled use of a vortex for capturing the working availability in the atmosphere (i.e., for the production of mechanical work). This mechanical work, produced from solar energy, could be obtained by ground level turbines.

In the previously mentioned papers, a vital part of the plant (the part that transforms solar energy into mechanical work) is the vortex flow structure. Ninić and Nižetić (2007) showed that in a solar chimney power plant with a short diffuser, the air is heated in the solar collector as in the SC power plant. Thus, a relatively tall concrete chimney could be replaced with a short one. The second concept proposed by Michaud (1995, 2005) is almost analogous to the previously mentioned concept. The difference between these two solutions is in the process of air heating. In Michaud's concept, the air is heated by waste industrial heat, while in Ninić's concept the air is heated by utilization of energy from the solar collector. A detailed overview of Michaud's concept was given in Ninić et al. (2009).

However, in Michaud (1995, 2005) and Ninić (2006), detailed physical and analytical formulations of the vortex stream structure were not elaborated, although they did appear in Ninić et al. (2009). This paper deals with a stationary vortex flow structure (as a part of the plant), which is called a GVC. For a simplified physical and analytical "three-layer" model of GVCs, a numerical simulation algorithm (GVC-simulator) has also been developed.

Hence, the objective of this paper is to further improve the elementary three-layer model of GVCs first proposed in Ninić et al. (2009). The introduced improvements are related to:

- variable vertical velocity in the central GVC updraft flow;
- the influence of the internal friction work;
- the reduction of the downdraft shell angular momentum.

These improvements will be introduced in the improved three-layer analytical model. Impact parameter analysis will also be performed in order to determine how the improvements affect the GVC flow structure.

2. Physical characteristics of the improved GVC model

As in the elementary GVC model (Ninić et al., 2009), we start from the assumption of stationary updraft airflow at the exit of a short chimney positioned over the turbines. The updraft has a spiraling upward flow. As a consequence, the pressure inside the flow structure is lower than the atmospheric

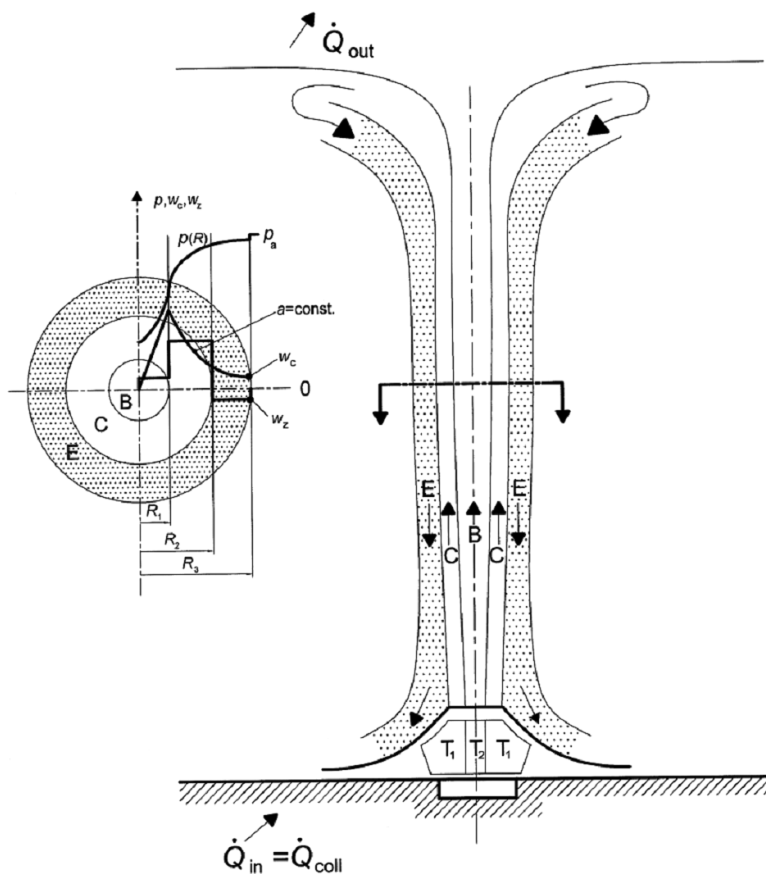


Figure 1. A simplified three-layer physical model of the GVC stationary vortex column, Ninić et al. (2009).

pressure at the same height. The structure of the elementary three-layer stationary model is illustrated in Fig. 1.

According to Fig. 1, the flow structure of the GVC consists of three characteristic sections: B, C, and E. Through the first GVC section ($R_1(z) > R(z) > 0$), the updraft (Fig. 1, airflow B) has a spiraling upward flow. According to the assumptions, this airflow is rotating as a solid body with respect to the “free vortex” law in Rankine’s terminology. This assumption was validated by field observations of natural vortex structures in Bluestein (2005). The second section of the GVC is annular rising flow C ($R_2(z) > R(z) > R_1(z)$), which is concentric with the central one (airflow B). Both airflows B and C originate from the equilibrium air collector adiabat (all air states inside the sections will be on this adiabat). The third GVC section is a characteristic downdraft shell, modeled as a cooled descending airflow, E.

In this paper, we did not analyze the structure of the downdraft shell; it is modeled as a black box. However, in the improved model we impose a parameter (the downdraft shell characteristic $\Pi_k(z)$) that characterizes this unknown downdraft shell structure.

The reason for supplementing the first proposed two-cell model with the three-layer model was explained in detail in Ninić et al. (2009). In the same paper, according to thermodynamic analysis of the two-cell model, it was concluded that the two-cell model cannot be the basis for realistic functioning GVC devices if sufficient heat rejection is not ensured. Specifically, the pressure gap, $p_a(0) - p_2(0)$, can only be bridged with sufficient heat rejection. This conclusion is the most important one because it ensures a sufficient quantity of turbine work. There are two possible means of heat rejection. The first is by the downdraft shell mechanism (cooled air downdraft, marked E in Fig. 1). The second way is provided by a weakly forced central downdraft of cold air in the central section of the GVC. The variant with the downdraft shell mechanism is analyzed in this paper.

A schematic overview of the profiles for three axially symmetric layers that are characterized by the pressure $p(z)$, circular velocity $w_c(z)$, vertical velocity $w_z(z)$, and by radii $R_1(z)$, $R_2(z)$, and $R_3(z)$ are also shown in Fig. 1.

In Ninić et al. (2009), the radial loss of angular momentum in the direction of the static atmosphere was neglected (the reason for this was discussed in section 5.0 of the same paper). In this improved model, radial loss of the downdraft shell angular momentum is reduced by a specified factor. This means that the possibility of radial loss of angular momentum at the downdraft shell periphery (because of side contact with standard atmosphere, as per NOAA, 1976) has been taken into account.

Internal friction is also taken into account with the unused part of working availability at the top of the GVC ($\Delta e_{coll\ tech}^{net}$) that was purposely left out. In this paper, the structure of the expression for the internal friction work, Δw_{fr} , was not worked out but the quantity of the unused part of the availability at the top of the GVC (which has been “reserved” for internal friction work) was varied in a simplified energy Eq. (1)¹. By doing this, the influence of internal friction on the physical values of the GVC is ensured.

$$-v\Delta p = \Delta e_p + \Delta e_k + \Delta w_{fr} \quad (1)$$

The starting assumptions, boundary conditions, and other physical circumstances are identical to those discussed for the elementary model in Ninić et al. (2009) (see sections 2 and 6). Thermodynamic validation of the proposed physical three-layer model with a downdraft annular shell was also provided

¹ Eq. (1) is written for the stream line along the annular updraft flow.

in the same paper (in section 4.2). Thus, the improved three-layer model is also validated by relying on the conclusions that were derived for the elementary three-layer model.

3. Analytical formulation

As in the case of the elementary GVC model, relations based on general principles of conservation of mass, momentum, and angular momentum, and the First Law of Thermodynamics where used.

The introduced improvements will be analytically formulated in the following section of this paper.

3.1. Variable vertical velocity at the central GVC section

The first improvement is related to the variability of velocity with height at the central GVC section, ${}^0\bar{w}_z^1(z)$. This vertical velocity is uniform along the radius at any distance from the ground in the section $R_1(z) > R(z) > 0$. If we apply the First Law of Thermodynamics for a specific streamline in the GVC axis (for two different thermodynamic observers, Nižetić (2009)) we can determine the vertical velocity, $w_0(z)$. In the first approximation, we assumed that the vertical velocity of the air in the GVC axis is approximately equal to the average vertical velocity at the central GVC section, i.e. $w_0(z) \cong {}^0\bar{w}_z^1(z)$. The First law of Thermodynamics, in its general form, is:

$$-v(z)dp(z) = de_p + de_k + dw_{\hat{r}} = g dz + w_z(z)dw_z(z) + w_c(z)dw_c(z) + dw_{\hat{r}}, \quad (2)$$

where e_p is the specific potential energy, e_k is the specific kinetic energy, $w_z(z)$ is the vertical velocity, $w_c(z)$ is the circular velocity and $w_{\hat{r}}$ is the internal friction work. Hence, if we apply Eq. (2) for a streamline in the GVC axis, it follows that:

$$-v(z)dp_0(z) = g dz + w_{z_0}(z)dw_{z_0}(z). \quad (3)$$

Eq. (3) with respect to Eq. (2) does not have the term related to internal friction work (because the friction is not present in the GVC axis), and the term for circular velocity is also eliminated (as a consequence of the Rankine free vortex law). By integration of Eq. (3), the distribution of vertical velocity with height on the central section of the GVC can be determined. After determination of the vertical velocity $w_{z_0}(z)$, a correction of the pressure in the GVC axis must be done. Namely, the pressure in the GVC axis, $p_0(z)$, must be lower due to the amount of kinetic energy expressed in the vertical velocity $w_{z_0}(z)$. Hence it follows that:

$$dp_0(z) = \rho_0(z)w_{z_0}(z)dw_{z_0}, \quad (4)$$

where $\rho_0(z)$ is the average density of air in the GVC axis from the equilibrium air collector adiabat (determined for specified t_{coll} and φ_{coll}). Therefore, in each

numerical step, the vertical velocity of air in the GVC axis (i.e., according to the approximation of its average value ${}^0\bar{w}_z^1(z)$) can be calculated from Eq. (3). After that, the pressure correction must be done according to Eq. (4).

In this procedure, the variation of vertical velocity with height in the GVC axis is also taken into account (which was not the case in the elementary GVC model, where this vertical velocity was assumed to be constant and negligible).

3.2. Quantity of internal friction work in the GVC flow structure

In this improved GVC model, internal friction work is treated in the zone of the annular updraft shell, $R_2(z) > R(z) > R_1(z)$, using the characteristic streamline on the radius $R_1(z)$. The amount of internal friction work dw_{fr} is ensured in Eq. (2). Hence, Eq. (2) applied to the streamline on the radius $R_1(z)$ is:

$$-v(z)dp_1(z) = g dz + w_{c_1}(z)dw_c(z) + w_{z_1}(z)dw_z(z) + dw_{fr}. \quad (5)$$

In section 5 of Ninić et al. (2009), the influence of internal friction work was analyzed in detail. In the same paper (see Fig. 10), the characteristic Mollier h - s diagram of the process in the GVC with a Brayton cycle was also shown. In this analysis, a certain amount of the unused part of the availability $\Delta e_{colltech}^{net}$ has been purposely left out as a “reserve” for the internal friction work Δw_{fr} . According to Fig. 10 from Ninić et al. (2009), for certain circumstances the analytical reserve for internal friction work can be obtained as:

$$w_{fr_re} = h_{12+} - h_{02}, \quad (6)$$

where $w_{fr_re} \equiv \Delta e_{colltech}^{net}$.

Hence, the available reserve for the internal friction work is calculated as an enthalpy difference of characteristic air states at the maximum available GVC height (the troposphere layer at z_{max}). In this improved model, the distribution of internal friction work is assumed to be linear (i.e., it is distributed linearly along the streamline on the radius $R_1(z)$ from the ground level to z_{max}). Hence, one part of the internal friction work is present in each numerical step depending on the value of the internal friction factor k_{fr} . In general, the internal friction work reduces the available part of the working availability $\Delta e_{colltech}^{net}$.

The quantity of internal friction work (in each height step) $\Delta w_{fr}(z)$ is defined by:

$$\Delta w_{fr}(z) = w_{fr_m} \cdot \Delta z \cdot k_{fr}, \quad (7)$$

where the internal friction work per meter of GVC height is:

$$w_{fr_m} = \frac{w_{fr_re}}{z_{max} - \Delta z_d}, \quad (8)$$

with the requirement that:

$$\sum_z \Delta w_{fr}(z) \leq w_{fr_re}. \quad (9)$$

The internal friction factor k_{fr} is introduced in Eq. (7). The reason for this lies in the possibility of investigating the magnitude of the effects of the internal friction work, k_{fr} , on the GVC's physical parameters. The degree of internal friction work utilization is introduced via the factor. μ_{fr} . It is defined as:

$$\mu_{fr} = \frac{\sum_z \Delta w_{fr}(z)}{w_{fr_re}} \leq 1, \quad (10)$$

where by using the factor μ_{fr} the amount of extracted internal friction work can be determined.

With this approach, the internal friction work is taken into account without elaboration of its structure.

3.3. Radial loss of downdraft shell angular momentum

In this improved model, radial loss of angular momentum is taken into account in a simplified way. In Ninić et al. (2009), the reasons for neglecting radial angular momentum dissipation were specified. However, it was also pointed out that the possibility of radial loss of angular momentum at the periphery of the downdraft shell exists (because of side contact with the atmosphere). So, in this improved and simplified model, radial loss of downdraft shell angular momentum is included using the parameter f . In this case, the downdraft shell angular momentum is:

$$a_k = f \cdot a, \quad (11)$$

where the parameter f represents the factor for reduction of the downdraft shell angular momentum. Thus, the downdraft shell angular momentum is always lower than (or equal to) the initial angular momentum ($a \leq a_k$).

3.4. Closed system of equations for the improved GVC model

In the closed system of equations for the elementary GVC model (see section 7.0 in Ninić et al., 2009), there were six unknown functions of height. In this improved model there is an additional differential equation, which is related to the variable vertical velocity at the central section of the GVC. Other improvements (internal friction and downdraft shell angular momentum) are also taken into account as extensions of the elementary GVC model's system of equations. Hence, with the known boundary conditions (which are analogous to those used in the elementary GVC model in Ninić et al., 2009) and with the introduced improvements, the closed differential equation system (with seven equations) can be formulated as follows:

I. First Law of Thermodynamics for central GVC section

$$-v(z)dp_0(z) = g dz + w_{z_0}(z)dw_{z_0}(z), \quad (12)$$

II. Angular momentum maintenance for annular updraft shell $R_1(z) < R(z) < R_2(z)$

$$w_c(z) \cdot R(z) = a = const, \quad (13)$$

III. Radial pressure equilibrium for radii interval $0 < R(z) < R_1(z)$

$$\int_0^1 w_c(z) dw_c + \int_0^1 v(p) dp = 0, \quad (14)$$

IV. Radial pressure equilibrium for radii interval $R_1(z) < R(z) < R_2(z)$

$$\int_1^2 w_c(z) dw_c + \int_1^2 v(p) dp = 0, \quad (15)$$

V. Mass flow conservation for central GVC section and for annular updraft shell

$$\dot{m}_{0-1} = {}^0\bar{\rho}^{-1}(p) {}^0\bar{w}_z^1(\Delta z_d) \int_0^1 2r dr \pi = const, \quad (16)$$

$$\dot{m}_{1-2} = {}^1\bar{\rho}^{-2}(p) {}^1\bar{w}_z^2(\Delta z_d) \int_1^2 2r dr \pi = const, \quad (17)$$

VI. First Law of Thermodynamics (written for two different observers) for annular updraft shell on the streamline on radius $R_1(z)$, (with $dw_{fr} \neq 0$)

$$-v(z)dp_1(z) = g dz + w_{c_1}(z)dw_c(z) + w_{z_1}(z)dw_z(z) + dw_{fr}, \quad (18)$$

$$\text{with } \Delta w_{fr}(z) = w_{fr_m} \cdot \Delta z \cdot k_{fr}, \quad (18a)$$

VII. Radial pressure equilibrium for downdraft shell in radii interval $R_2(z) < R(z) < R_2(z) + \delta_k(z)$

$$\int_2^a dp_a = \Pi_k(z) \cdot \frac{(f \cdot a)^2}{R_2(z)^3}, \quad (19)$$

where ${}^0\bar{\rho}^{-1}(p) {}^1\bar{\rho}^{-2}(p)$ are average densities of air and ${}^0\bar{w}_z^1(z), {}^1\bar{w}_z^2(z)$ are average vertical velocities in characteristic sections of the GVC. The factor $\Pi_k(z)$ represents the downdraft shell characteristic, which is equal to the product of the effective density and the thickness of the downdraft shell (in each numerical height step), i.e., $\Pi_k(z) = \rho_k(z) \cdot \delta_k(z)$.

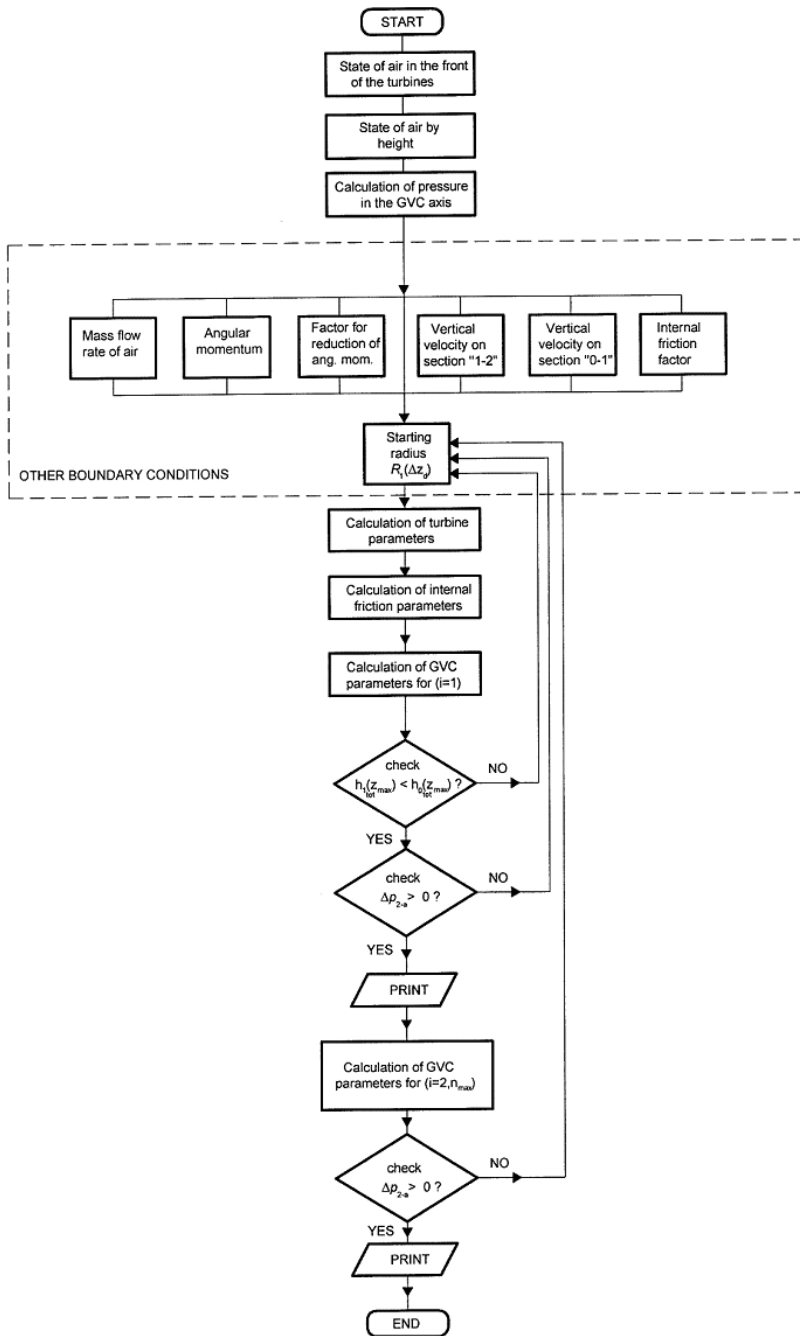


Figure 2. Flowchart for improved GVC simplified model.

If the above system of equations is solved, the physical values of state (for the improved GVC model) can be obtained for an arbitrary height step. In the remainder of this paper, the algorithm for the two-dimensional improved GVC model is given together with a characteristic numerical solution.

4. An algorithm and characteristic numerical solution

4.1. Flowchart for numerical simulation algorithm

For the purpose of this analysis, a computer simulation program has also been developed. A flowchart of the improved GVC simulation algorithm is shown in Fig. 2.

The start of the program considers the state of air in front of the turbines (t_{coll} and φ_{coll}). Then, the program computes the equilibrium air collector adiabat (i.e., the calculation of air properties by height, $\rho(z)$, $p(z)$ and the calculation of pressure in the GVC axis). The program then proceeds with the definition of the starting radius (at the level of the short chimney outlet) $R_1(\Delta z_d)$ and continues with the calculation of the GVC values of state in the first numerical step ($i = 1$). In the same numerical step, the turbine parameters (total turbine power and heat to work efficiency) are also calculated. Then the program checks the satisfactions of two specific conditions, $h_{0_{tot}} < h_{0_{tot}}$ (this condition ensures working availability for internal friction work) and $\Delta p_{2-a} > 0$ (fulfillment of downdraft shell radial pressure equilibrium). If the conditions are satisfied, the internal friction parameters $w_{fr, re}$, $w_{fr, m}$ and μ_{fr} are calculated. The program continues to the second numerical step ($i = 2$), where (according to the presented and improved analytical GVC model) values of state (properties) in the GVC are calculated for an arbitrary height (if the above-mentioned specified conditions are fulfilled). The program stops when the troposphere height level (z_{max}) is reached.

4.2. Characteristic numerical solution

To calculate the physical properties of the improved GVC model, it is necessary to define the boundary conditions at the height level of the short chimney outlet Δz_d . Hence, the boundary conditions are:

- total mass flow rate of air: $m_a = 9\,500$ [kg/s],
- angular momentum: $a = 400$ [m²/s],
- uniform vertical velocity at central GVC section: ${}^0\bar{w}_z^1 = 35$ [m/s],
- uniform vertical velocity of annular updraft shell: ${}^1\bar{w}_z^2 = 35$ [m/s],
- parameter for reduction of downdraft shell angular momentum: $f = 15$ [%],
- temperature of air at the collector outlet: $t_{coll} = 45.0$ [°C],
- relative humidity of moist air: $\varphi_{coll} = 30.0$ [%],
- starting radius: $R_1(\Delta z_d) = 7.0$ [m],
- internal friction factor: $k_{fr} = 0.3$

Table 1. State values by height

BOUNDARY CONDITIONS												
R_{poc} (m)	a (m^2/s)	w_{yp0I} (m/s)	w_{yp12} (m/s)	m_{uk} (kg/s)	f (%)							
7	400	35	35	9 500	15							
TURBINES AND DOWN-STREAM PARAMETERS:												
h_{00} (J/kg)	h_{01} (J/kg)	h_{01+} (J/kg)	h_{11} (J/kg)	h_{11+} (J/kg)	h_{02} (J/kg)	h_{12+} (J/kg)						
92 192	79 769	80 382	81 366	83 611	-15326	-14390						
w_p (J/kg)	w_o (J/kg)	P_p (MW)	P_o (MW)	Q_d (MW)	P_t (MW)	h (%)						
8 580	10 195	36.444	53.555	732.612	89.999	12.28						
PARAMETERS OF INTERNAL FRICTION:												
w_{fr} (J/kg)	P_{fr} (MW)	k_{fr}										
3 229	13.71	0.3										
PROPERTIES OF HEATED MOIST AIR AT THE COLLECTOR OUTLET:												
t (°C)	j (%)	x (g_w (kg $_Z$))										
45.0	30	18.2										
SIMULATION RESULTS:												
H(m)	R_1 (m)	R_2 (m)	p_0 (bar)	p_1 (bar)	p_2 (bar)	P_{at} (bar)	w_{y0} (m/s)	w_{y12} (m/s)	w_{e1} (m/s)	w_{e2} (m/s)	Π_k (kg/m 2)	p_1-p_2 (hPa)
10	7.00	9.33	0.882	0.699	0.906	1.012	35.0	35.0	57.1	42.8	74.8	106.2
200	6.99	8.78	0.858	0.874	0.88	0.989	35.1	48.2	57.2	45.5	63.9	109.1
400	7.03	8.64	0.840	0.655	0.861	0.966	35.2	48.1	56.8	45.2	62.9	105.0
600	7.08	8.91	0.821	0.836	0.842	0.943	35.3	48.0	56.4	44.8	61.9	101.1
800	7.13	8.98	0.803	0.818	0.823	0.921	35.4	47.9	56.0	44.5	60.9	97.3
1 000	7.20	9.04	0.876	0.800	0.805	0.899	35.7	48.3	55.5	44.2	60.1	93.8
1 500	7.06	9.13	0.742	0.756	0.761	0.846	38.7	45.3	56.5	43.8	55.4	84.1
2 000	6.90	9.21	0.700	0.713	0.720	0.795	43.0	42.4	57.9	43.4	51.0	75.2
3 000	6.50	9.44	0.620	0.634	0.642	0.701	53.3	37.1	61.4	42.3	43.4	59.5
4 000	6.33	9.52	0.548	0.561	0.559	0.616	62.2	36.1	63.0	41.9	35.7	47.7
5 000	6.29	9.43	0.482	0.495	0.502	0.540	70.2	43.5	63.5	42.3	28.0	38.5
6 000	6.32	9.32	0.424	0.435	0.441	0.472	77.4	51.1	63.2	42.8	21.7	31.0
7 000	6.40	9.28	0.371	0.381	0.386	0.411	84.0	59.6	62.4	43.0	17.0	24.6
8 000	6.53	9.32	0.324	0.332	0.337	0.356	90.2	68.5	61.2	42.9	13.5	19.3
9 000	6.70	9.43	0.282	0.289	0.293	0.307	94.3	77.0	59.6	42.3	10.7	4.7
9 400	6.81	9.55	0.267	0.274	0.277	0.290	95.2	79.4	58.6	41.8	9.7	12.8
9 800	6.92	9.68	0.252	0.259	0.261	0.273	95.9	81.9	57.7	41.3	8.7	11.1
10 000	inf.	inf.	0.264	0.264	0.264	0.264	0.0	0.0	0.0	0.0	0.0	0.0

USED PART OF AIR WORKING AVAILABILITY FOR INTERNAL FRICTION (J/kg): 949
 AVAILABLE RESERVE FOR INTERNAL FRICTION WORK (J/kg): 3229
 UTILIZED PART OF RESERVE FOR INTERNAL FRICTION WORK (%): 29,4

Analogous to those in the elementary GVC model, the values of state at an arbitrary height step are calculated for the given boundary conditions. Numerical simulation of the improved GVC model has been provided by the previously described numerical model. Results of this simulation for a characteristic numerical solution are given in Table 1, together with a legend for each label description.

4.3. Discussion of numerical results

The geometries of the elementary and improved GVC models are shown together in Fig. 3. (i.e., the characteristic radii $R_1(z)$ and $R_2(z)$ are shown). The solid curve shows the improved GVC model, and the dashed curve shows the elementary model. In the interest of clarity, only one half of the axisymmetrical GVC flow is shown in Fig. 3. Although the starting boundary conditions are not identical for both models, the comparison of results has been provided for useful conclusions that will be addressed in the discussion section of this paper. The reason for using different starting boundary conditions is to achieve the optimal case when the GVC structure reaches the top of the troposphere layer.

Similar to the case in the elementary three-layer model, the GVC geometry of the improved model is increased by the elevation of the warm moist air. The starting radius at the level of the short chimney outlet $R_1(\Delta z_d) = 7.0$ m, and its value is lower than in the elementary model ($R_1(\Delta z_d) = 10.2$ m). A lower value of the radius $R_1(\Delta z_d)$ was necessary to obtain the optimal case where the GVC reaches the top of the troposphere layer. The characteristic GVC radii $R_1(\Delta z)$ and $R_2(\Delta z_d)$ increase more slowly with height compared to the elementary model. In addition, the range between these two radii in numerical steps is lower than that in the elementary model. At the troposphere height level in both models, the geometry turns into a characteristic “mushroom”. In general, this shape resembles the geometry of natural vortex structures. There are also zones in the GVC where the values of characteristic radii decrease slightly with height (which is not the case with the elementary model). The reason for this lies in the fact that in this improved GVC model, the work of internal friction and variable vertical velocity are taken into account.

The radial pressure profile in section A–A (which corresponds to a numerical/height step of $z = 2\,000$ m) is shown in Fig. 4 for circumstances according to the Table 1. The radial pressure profile of the elementary model is also shown in the same figure.

Data that relate to the elementary model are shown as a dashed curve, and data from the improved model are shown as a solid curve. According to the characteristic numerical solution, pressure in section A–A increases along the radius, from the pressure in the GVC axis, $p_0(2\,000) = 0.700$ bar, to a pressure of $p_1(2\,000) = 0.713$ bar, which corresponds to a radius of $R_1(2\,000) = 6.90$ m. Furthermore, in the annular updraft shell, pressure increases from a pressure of $p_1(2\,000)$ on $R_1(2\,000)$ to a pressure of $p_2(2\,000) = 0.720$ bar on the radius

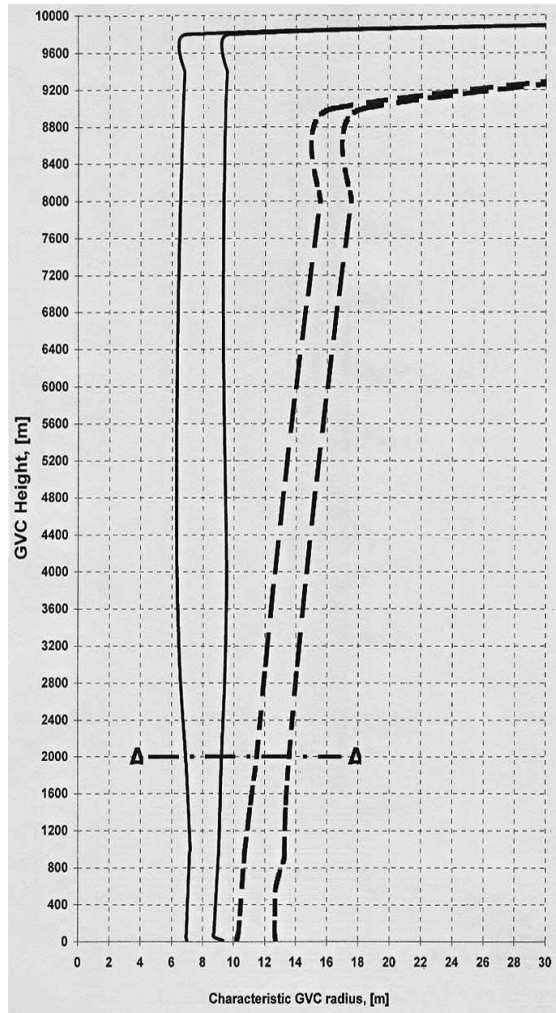


Figure 3. Comparison between the GVC geometry of elementary and improved simplified models.

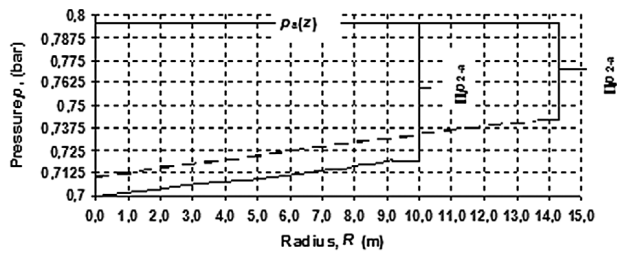


Figure 4. Comparison of radial profiles for elementary and improved models in section A-A.

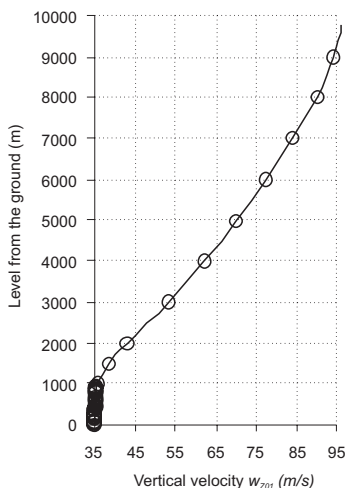


Fig. 5. Height distribution of vertical velocity at central GVC section ${}^0\bar{w}_z^1(z)$.

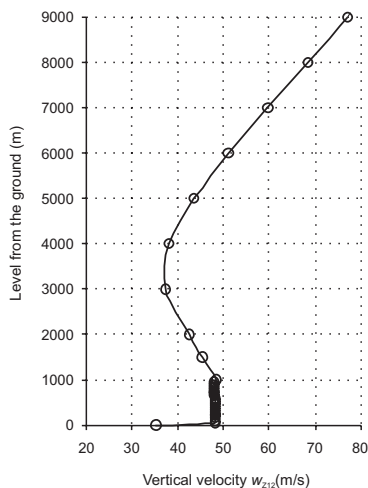


Figure 6. Height distribution of vertical velocity for annular updraft shell ${}^0\bar{w}_z^1(z)$.

$R_2(2\ 000) = 9.21$ m. The atmospheric pressure profiles $p_a(z)$ are identical in both models (standard atmosphere). The pressure growth trend in the improved model is somewhat similar to the pressure trend in the elementary model. The first difference between pressure trends is in the lower value of pressure in the GVC axis in the improved model, as shown in Fig. 4. The lower value of pressure in the GVC axis is due to the influence of vertical velocity ${}^0\bar{w}_z^1(\Delta z_d)$. The second difference is the greater pressure difference $\Delta p_{2-a}(z)$ in the improved model (as a consequence of the downdraft shell reducing factor f).

The variation of the average vertical velocity of air at the central GVC section is shown in Fig. 5. The vertical velocity ${}^0\bar{w}_z^1(z)$ is almost constant up to the GVC height of ≈ 1 km. After that, the vertical velocity (see Fig. 5) has a constant growth until the maximum GVC height (level z_{\max}) is reached (the distribution of velocity ${}^0\bar{w}_z^1(z)$ in Fig. 5 is shown to a GVC height of 9.5 km, because after reaching the level of z_{\max} , according to the model assumptions, all velocities disappear).

Figure 6 represents the height profile of the vertical velocity of the annular upward shell ${}^1\bar{w}_z^2(z)$. For the chosen numerical solution, the vertical velocity ${}^1\bar{w}_z^2(z)$ is almost constant to a GVC height of ≈ 1 km (except for the step near ground level).

After that there is a constant decrease until a height of ≈ 4 km. Then the vertical velocity has a constant growth until a height of ≈ 9.5 km. This dynamical trend in vertical velocity ${}^1\bar{w}_z^2(z)$ is a consequence of the internal friction work.

Radial profiles of circular velocities for both models are shown in Fig. 7. Although the initial angular momentum of the simplified model ($a = 600 \text{ m}^2/\text{s}$) is greater than that in the improved model ($a = 400 \text{ m}^2/\text{s}$), the maximum circular velocity is greater in the improved model because of the lower starting value of radius $R_1(\Delta z_d)$. As was previously mentioned, the reason for the lower starting radius $R_1(\Delta z_d)$ is due to the introduced improvements in the three-layer model. The maximum circular velocity for the characteristic numerical solution is $w_{c1\max} = 57.9 \text{ m/s}$ on the radius $R_1(2\ 000)$ (in meteorology, this radius is called the radius of maximum wind).

The resultant turbine power for the numerical example is approximately equal to $\approx 90 \text{ MW}$, with a heat to work efficiency of 12.3 %. This means that heat input in the collector (from the solar radiation) must be about $\approx 731 \text{ MW}$. As expected, the resultant turbine power of the improved model is greater than that in the elementary model, due to the different starting boundary conditions. The improved algorithm gives theoretical powers as follows: ${}^0\bar{P}_t^1 = 53.5 \text{ MW}$ for central turbines and ${}^1\bar{P}_t^2 = 36.4 \text{ MW}$ for peripheral turbines. It is obvious that for this example, much more power can be utilized from the central turbines. The reason for higher central turbine power lies in the higher vertical velocity ${}^0\bar{w}_z^1(\Delta z_y)$ that is necessary to overcome the influence of internal friction.

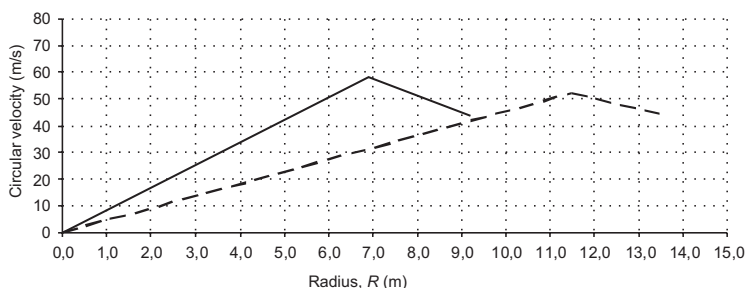


Figure 7. Comparison of radial profiles in the GVC section A–A.

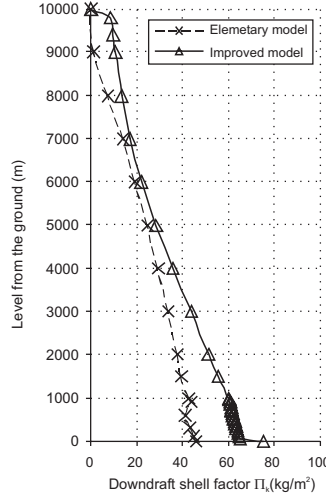


Figure 8. Comparison of downdraft shell characteristic $\Pi_k(z)$.

Namely, due to higher vertical velocity in the central GVC section, the partial mass flow rate of air m_{0-1} is also increased. In this numerical example, the power that has been spent to overcome the internal friction work is $P_{fr} = 13.71$ MW, with an internal friction factor of $k_{fr} = 0.3$. The degree of internal friction work utilization is $\mu_{fr} = 29.4$ %, which corresponds to a used working availability of 949.3 J/kg.

The height distribution of the downdraft shell characteristic is shown in Fig. 8 for both models. In the numerical solution of the improved GVC model, a higher numerical value of $\Pi_k(z)$ is obtained when comparing the solution with the elementary model. This higher $\Pi_k(z)$ value is due to the reduction of the downdraft shell angular momentum a_k by the factor.

Furthermore, the $\Pi_k(z)$ function continuously and slightly decreases with increases in GVC height (which is not the case in the elementary model, where the decrease in height is slightly more emphasized). As in the case of the elementary model, the $\Pi_k(z)$ function has the largest value at the ground level ($\Pi_k(z) = 74.8$ kg/m²) and decreases with GVC height. Upon reaching the GVC top at z_{max} , the $\Pi_k(z)$ function disappears.

5. Conclusion

Further development of a proposed elementary stationary three-layer model of GVCs is provided in this paper. Improvements that are related to the variable vertical velocity in the central GVC section, and also to internal friction work, are involved in this simplified three-layer model. The reduction factor of downdraft shell angular momentum is also introduced in this simplified

model. With this factor, the possibility of air mixing with the surrounding atmosphere at the periphery of the downdraft shell is taken into account.

A typical numerical solution is given for the boundary conditions, together with the introduced parameters in this improved model. In order to achieve the optimal case (where the GVC height would be equal to the thickness of the troposphere level), the starting boundary conditions were not the same as those in the elementary model.

According to the typical numerical solution presented in this paper, the GVC geometry (with respect to the geometry of the elementary model) generally shows different radii trends by height. Namely, the characteristic GVC radii of the improved model both increase and decrease in arbitrary numerical height steps. That radial trend is created by vertical velocity changes in the annular updraft flow, according to Fig. 6. In the elementary GVC model this was not the case, because the radii continuously increased with increases in GVC height. Hence, it can be concluded that the strongest influence on the characteristic radius of the GVC geometry $R_1(\Delta z)$ is a variable velocity in the central GVC section, ${}^0\bar{w}_z^1(z)$ (which is expected from the conservation of mass on the central GVC section). Furthermore, the most influential parameter on the radius $R_2(z)$ is the internal friction factor k_{fr} (which influences the annular updraft shell vertical velocity ${}^1\bar{w}_z^2(z)$).

As expected, the factor for the reduction of the downdraft shell angular momentum, f_β , has the most significant influence on the downdraft shell characteristic $\Pi_k(z)$. Hence, in this improved model, a greater pressure difference Δp_{2-a} is necessary (in order to satisfy the radial pressure equilibrium of the downdraft shell), compared to the radial pressure difference in the elementary model.

The resultant turbine power and heat to work efficiency are most affected by the change of the air state at the collector outlet. This change is primarily due to the relative humidity of warm collector air. An increase in relative humidity causes the increase in resultant turbine power and heat to work efficiency. Slightly less influence on the resultant turbine power and heat to work efficiency is seen from the vertical velocity at the central GVC section and the total mass flow rate of air.

Finally, it can be concluded that the introduced improvements to the elementary three-layer model have the most significant influence on the GVC properties. Thus, this kind of analysis was necessary and is also useful for further development of the model.

Acknowledgements – Author would like to thank the Croatian Ministry of Science, Education and Sports for funding this project (023-0231751-3011).

Nomenclature

a [m ² /s]	– angular momentum
a_k [m ² /s]	– downdraft shell angular momentum

e_k [J/kg]	– specific kinetic energy
e_p [J/kg]	– specific potential energy
$e_{colltech}^{net}$ [J/kg]	– the net technically feasible part of energy or height potential
f	– downdraft shell reduction factor
g [m ² /s]	– gravitational acceleration
h [J/kg]	– specific enthalpy of air
k_{fr}	– internal friction factor
\dot{m}_a [kg/s]	– total mass flow rate of air
\dot{m}_{0-1}	– mass flow rate through the internal GVC layer
\dot{m}_{1-2}	– mass flow rate through the GVC updraft shell
p [Pa]	– pressure
R [m]	– radius
t [°C]	– temperature
v [m ³ /kg]	– specific volume of air
z [m]	– level from the ground
w_i [J/kg]	– specific shaft work
w_c [m/s]	– circular velocity
w_{fr} [J/kg]	– specific internal friction work
w_z [m/s]	– vertical velocity
w_{fr-re} [J/kg]	– reserved availability for internal friction work
w_{fr-m}	– internal friction work per meter of GVC height
${}^0\bar{w}_z^1$	– vertical velocity of the internal GVC layer
${}^1\bar{w}_z^2$	– vertical velocity of the GVC updraft shell
z_{max} [m]	– maximum height
δ_k [m]	– thickness of the GVC downdraft shell
Δz [m]	– height step
Δz_d [m]	– height at the short chimney outlet
η_t	– heat to work efficiency
μ_{fr}	– degree of internal friction work utilization
$\Pi_k(z)$ [kg/m ²]	– characteristic of the downdraft shell
ρ [kg/m ³]	– density of air
φ	– relative humidity of air

Subscripts:

0	– axis
a	– atmospheric
c	– circular (component) velocity
coll	– collector
k	– kinetic energy
p	– potential energy

- z – component of vertical velocity
 1 – at radius $R_1(z)$
 2 – at radius $R_2(z)$

Double subscripts:

- 02 – state in the axis at $z = 10\ 000$
 12 – state at radius R_1 , $z = 10\ 000$

Superscripts:

- + – stagnation state without w_c and with w_z
 fr – internal friction

References

- Bernardes, M. A. S, Voß, A. and Weinrebe, G. (2003): Thermal and technical analyses of solar chimneys, *Sol. Energy*, **75**, 511–524.
- Bilgen, E. and Rehault, J. (2005): Solar chimney power plants for high latitudes, *Sol. Energy*, **79**, 449–458.
- Bluestein, H. B. (2005): A review of ground-based, mobile, W-band Doppler-radar observations of tornadoes and dust devils, *Dynam. Atmos. Oceans*, **40**, 163–188.
- Dessoliers, H. (1913): Comment l'homme accroit progressivement les pluies des régions arides, Refoulement du Sahara, Alger.
- Dessens, J. (1962): Man-made tornadoes, *Nature*, **193**, 13–14.
- Dessens, J. (1969): Etude des vortex du type tornado á partir de modeles de laboratoire, Thesis, University of Paris.
- Haff, W. (1984): Solar chimneys, part II: preliminary test results from the Manzanares pilot plant, *Int. J. Solar Energy*, **2**, 141–161.
- Haff, W., Friedrich, K., Mayr, G. and Schlaich, J. (1983): Solar chimneys. Part I: Principle and construction of the pilot plant in Manzanares, *Int. J. Sol. Energy*, **2**, 3–20.
- Michaud L. M. (1975): Proposal for the use of a controlled tornado-like vortex to capture the mechanical energy produced in the atmosphere from solar energy, *Bull. Amer. Meteor. Soc.*, **56**, 530–534.
- Michaud, L.M. (1995): Heat to work conversion during upward heat convection, Part I: Carnot engine method, *Atmos. Res.*, **39**, 157–178.
- Michaud, L.M. (1996). Heat to work conversion during upward heat convection, Part II: Internally generated entropy method, *Atmos. Res.*, **41**, 93–108.
- Michaud, L. M. (1999): Vortex process for capturing mechanical energy during upward heat-convection in the atmosphere, *Appl. Energ.*, **62**, 241–251.
- Michaud, L. M. (2005): Atmospheric Vortex Engine, <http://www.vortexengine.ca/>
- Ninić, N. (2006): Available energy of the air in solar chimneys and the possibility of its ground-level concentration, *Sol. Energy*, **80**, 804–811.
- Ninić, N., Jurić Z. and Nižetić S. (2006): Thermodynamical aspect of definitions CAPE and TCAPE, *Geofizika*, **23**, 143–154.
- Ninić, N. and Nižetić, S. (2009): Elementary theory of stationary vortex columns for solar chimney power plants, *Sol. Energy*, **83**, 462–476.
- Ninić, N. and Nižetić, S. (2007): Solar power plant with short diffuser, *Patented invention*. PCT/HR2007/000037.

- Nižetić, S.. (2009): Thermodynamical model of ground level energy concentration of warm humid air, PhD dissertation, FESB-Split, 194. pp.
- Nižetić, S., Ninić, N. and Klarin, B. (2009): Analysis and feasibility of implementing solar chimney power plants in the Mediterranean region, *Energy*, **33**, 1680–1690.
- Nižetić S. and Ninić N. (2007): Analysis of overall solar chimney power plant efficiency, *Strojarsstvo*, **49**, 233–240.
- Nižetić S. and Klarin B. (2009): A simplified analytical approach for evaluation of the optimal ratio of pressure drop across the turbine in solar chimney power plants, *Appl. Energ.*, **87**, 587–591.
- Padki, M. M. and Sherif, S. A. (1989): Solar chimney for medium-to-large scale power generation. *In: Proceedings of the Manila International Symposium on the Development and Management of Energy Resources*, Manila, Philippines, **1**, 432–437.
- Schlaich, J. (1995): *The solar chimney: Electricity from the sun*, Geislingen: Maurer C., Stuttgart, 55. pp.
- Von Backström, T. W. and Fluri T. P. (2006): Maximum fluid power condition in solar chimney power plants – An analytical approach, *Sol. Energy*, **80**, 1417–1423.
- NOAA/NASA/USAF, (1976): US Standard atmosphere 1976, Washington, DC.

SAŽETAK

Atmosferski gravitacijski vrtložni stup kao protočni objekt: poboljšanje troslojnog modela

Sandro Nižetić

U ovom radu razvijen je poboljšani troslojni analitički model gravitacijskog vrtložnog stupa (GVS) za solarne termoelektre. U suštini, razvijeni model predstavlja daljnje poboljšanje troslojnog modela predloženog u Ninić i ostali (2009). Uvedena poboljšanja u troslojni model odnose se na uvođenje utjecaja rada unutarnjeg trenja, promjenjive vertikalne brzine (s visinom) u centralnom dijelu GVS-a te na utjecaj promjenjivog momenta količine gibanja u spusnoj ljušci. Prikazano je karakteristično numeričko rješenje poboljšanoga modela i uspoređeno je s rješenjem dobivenim osnovnim modelom. Numerički rezultati pokazuju da uvedena poboljšanja predstavljaju važne parametre za daljnju analizu gravitacijskih vrtložnih stupova.

Ključne riječi: gravitacijski vrtložni stup, solarni dimnjak, numeričko modeliranje

Corresponding author's address: Sandro Nižetić, Rudera Boškovića bb, 21000 Split, Republic of Croatia, tel: 00385-1-305-948, fax: 00385-21-305-954, e-mail: snizetic@fesb.hr